Empirically Determined Auroral Electron Events at Mars-MAVEN Observations

Shaosui Xu, David L. Mitchell, James P. Mcfadden, Nicholas M. Schneider, Zachariah Milby, Sonal Jain, Tristan Weber, David A. Brain, Gina A. Dibraccio, Jasper Halekas, et al.

AGU ADVANCING EARTH AND SPACE SCIENCE

Geophysical Research Letters®

RESEARCH LETTER
10.1029/2022GL097757

Key Points:

- We establish empirical criteria to select electron events that could trigger detectable auroral observations
- We find similar statistical behaviors in selected electron events as discrete auroral events and explore the cause of statistical trends
- This study bridges the gap of these two types of observations and motivates collaborations across different Mars missions

Supporting Information:

Supporting Information may be found in the online version of this article.

Correspondence to:

S. Xu,
shaosui.xu@ssl.berkeley.edu

Citation:

Xu, S., Mitchell, D. L., McFadden, J. P., Schneider, N. M., Milby, Z., Jain, S., et al. (2022). Empirically determined auroral electron events at Mars—MAVEN observations. *Geophysical Research Letters*, *49*, e2022GL097757. https://doi.org/10.1029/2022GL097757

Received 5 JAN 2022
Accepted 17 MAR 2022

Empirically Determined Auroral Electron Events at Mars—MAVEN Observations

Shaosui Xu[1], David L. Mitchell[1], James P. McFadden[1], Nicholas M. Schneider[2], Zachariah Milby[2], Sonal Jain[2], Tristan Weber[2,3], David A. Brain[2], Gina A. DiBraccio[3], Jasper Halekas[4], Suranga Ruhunusiri[4], Christian Mazelle[5], Robert J. Lillis[1], and Ben Johnston[2]

[1]Space Sciences Laboratory, University of California, Berkeley, Berkeley, CA, USA, [2]Laboratory for Atmospheric and Space Physics, University of Colorado Boulder, Boulder, CO, USA, [3]Goddard Space Flight Center, Greenbelt, MD, USA, [4]Department of Physics and Astronomy, University of Iowa, Iowa City, IA, USA, [5]IRAP, CNRS, CNES, University of Toulouse – UPS, Toulouse, France

Abstract Discrete aurorae have been observed at magnetized planets such as Earth and Jupiter, triggered by accelerated electrons. Similar aurorae have also been observed at Mars with only localized strong crustal magnetisms. However, our understanding of this phenomenon at Mars is still limited. In particular, direct and quantitative comparisons of the auroral and its source electron events are lacking as these two types of observations are usually made at different times and/or locations. In this study, we establish empirical criteria to select electron events ("auroral electrons") that could trigger detectable auroral emissions with Mars Atmosphere and Volatile EvolutioN measurements, thereby enabling a direct statistical comparison. We find auroral electrons share similar statistical characteristics to those previously reported for discrete auroral events. This study bridges the gap between electron observations and auroral detections and enables collaborations across different Mars missions, as well as comparative planetary studies of discrete aurora.

Plain Language Summary Aurorae have been observed in the polar regions at magnetized planets such as Earth and Jupiter, triggered by accelerated electrons. Similarly, localized auroral emissions have also been reported at Mars with no global dipole field but localized strong crustal magnetisms. However, our understanding of aurorae at Mars is still very limited in terms of their characteristics and the source electrons. In particular, direct and quantitative comparisons of the auroral and electron events are lacking as these two types of observations are usually made at different times and/or locations because of the limitation of single-spacecraft observations. This study establishes empirical criteria to select auroral electrons and statistically compare these two types of observations. This study bridges the gap between the electron observations and auroral detections and enables collaborations across different Mars missions, as well as studies of auroral phenomena at different planets.

1. Introduction

The first report of auroral observations at Mars was made by Bertaux et al. (2005) using images from the Spectroscopy for Investigation of Characteristics of the Atmosphere of Mars (SPICAM) onboard Mars Express (MEx). The auroral events observed by MEx are localized and mostly concentrated around Mars' southern strong crustal magnetic fields (e.g., Leblanc et al., 2006, 2008). Later on, similar localized aurorae, termed "discrete aurora" at Mars, were observed with the imaging ultraviolet spectrograph (IUVS) instrument (McClintock et al., 2015) onboard the Mars Atmosphere and Volatile EvolutioN (MAVEN) spacecraft (e.g., Schneider et al., 2018). Recently, discrete auroral observations were also made by the United Arab Emirates' Hope spacecraft (https://www.nature.com/articles/d41586-021-01811-4). These discrete auroral events have been associated with localized electron acceleration events, based on similar geographic locations (e.g., Brain et al., 2006) and/or close-in-time observations of both type of events (e.g., Gérard et al., 2015; Leblanc et al., 2008; Xu, Mitchell, et al., 2020), similar to discrete auroral observations made at Earth (e.g., Birn et al., 2012) and Jupiter (Mauk et al., 2017). Most recently, Schneider et al. (2021) provide a statistical analysis of discrete auroral events observed by IUVS and reveal the preference of events near strong crustal fields for the evening hours and also westward upstream interplanetary magnetic fields (IMF).

While there have been studies suggesting that unaccelerated electrons with fluxes peaking at 20–30 eV (e.g., unaltered solar wind electrons or ionospheric photoelectrons) could trigger localized auroral emissions (e.g., Leblanc et al., 2006; Liemohn et al., 2006), more detailed characterizations of auroral events with simulations (e.g., Soret et al., 2016, 2021), particularly with the altitude profile of the emission, reveal that detectable auroral emissions require sufficient electron fluxes at high energies (~50–2,000 eV) to produce a peak emission at 100–150 km altitudes. Also, depending on the detection threshold and sensitivity of the remote-sensing instrument, similarly, a threshold should be applied to the electron flux to select source electrons. Nominal nightside precipitating solar wind electron fluxes (below ~400 km altitude) are observed to be lower than that in the upstream solar wind by both Mars Global Surveyor (MGS)(e.g., Mitchell et al., 2001; Shane et al., 2016) and MAVEN (e.g., Weber et al., 2017), which is caused by an accumulative deceleration by the ambipolar electric fields within the induced magnetosphere (Xu, Mitchell, et al., 2021). There are also dayside ionospheric photoelectrons transported and precipitating to the nightside via cross-terminator closed field lines (e.g., Xu, Mitchell, et al., 2016; Xu, Mitchell, Liemohn, et al., 2017; Xu, Mitchell, Luhmann, et al., 2017). As discrete aurorae are not highly frequently detected by SPICAM (only ~20 detections in total) or IUVS (an observational frequency of $>1\% - 4\%$), it implies nominal nightside precipitating electrons do not have sufficient energy and/or fluxes to cause detectable auroral emission. Indeed, as shown later, the flux of these precipitating electrons normally does not surpass the flux threshold determined in this study. It is also worth noting that, considering typical magnetic field line geometries, magnetosheath electrons with intense fluxes mostly observed near the subsolar region, accelerated by the cross-shock potential (e.g., Horaites et al., 2021; Schwartz et al., 2019; Xu, Schwartz, et al., 2021), do not usually have access to the nightside atmosphere and thus are not a direct source for discrete auroral emissions.

To trigger detectable auroral emission, some mechanisms/processes to enhance the high-energy (~50–2,000 eV) electron fluxes are needed, which could be either nominal precipitating electrons being accelerated within the Mars magnetosphere/ionosphere and/or enhanced upstream solar wind electron fluxes. Electron acceleration events at Mars have been identified with measurements from MGS (e.g., Brain et al., 2006; Halekas et al., 2008), MEx (e.g., Leblanc et al., 2008), and MAVEN (e.g., Akbari et al., 2019; Xu, Mitchell, et al., 2020). The acceleration mechanisms include, but are not limited to, narrow electrostatic potential layers within double-layers (associated with inverted-V electron events) (e.g., Brain et al., 2006; Xu, Mitchell, et al., 2020), acceleration associated with current sheet crossings (e.g., Halekas et al., 2008; Harada et al., 2020), and wave-particle interaction (e.g., Fowler et al., 2020, 2021). Meanwhile, upstream solar wind electron fluxes can be significantly increased during solar transient events such as interplanetary coronal mass ejections and stream interaction regions (e.g., Xu, Curry, et al., 2020). For such periods, additional electron acceleration might not be needed to produce detectable aurorae. It is worth mentioning that diffuse aurorae have been reported to be produced by SEP (solar energetic particle) electrons (energies above ~100 keV) (Schneider et al., 2015) but later reckoned to be produced by precipitating SEP protons by Nakamura et al. (2022). In contrast, it has been speculated that the hotter upstream solar wind sub-keV electrons could be a source for auroral emission but it is not yet confirmed by studies to our knowledge, partly because of the unknown electron flux threshold. It is important to discern the electron source of discrete aurorae at Mars to be properly compared with discrete aurorae at other magnetized planets. At Earth and Jupiter, discrete aurorae are particularly associated with broadband electron acceleration as a consequence of wave-particle interactions or inverted-V electron acceleration events (e.g., Birn et al., 2012; Mauk et al., 2020). In comparison, at Mars, discrete aurorae are defined as localized emission events. This localness may be a result of complex magnetic topology, if the electron source is hotter upstream solar wind electrons, rather than locally accelerated electrons.

While there have been case studies of combining discrete auroral observations with close-by electron acceleration events (e.g., Gérard et al., 2015; Leblanc et al., 2008; Soret et al., 2016, 2021), a systematic comparison of these two types of observations has been in lack, largely due to the difficulty of determining the threshold of electron fluxes to trigger observable auroral emissions. This also means the relative contribution of the two possible electron sources (locally accelerated vs. hotter upstream electrons) to the observed auroral emission cannot be determined either. In this study, we establish empirical criteria for selecting such source electron events (or "auroral electrons") with measurements from the Solar Wind Electron Analyzer (SWEA, Mitchell et al., 2016) onboard MAVEN in Section 2. By applying such criteria to the entire MAVEN mission, we statistically analyze these electron events and compare the statistical characteristics of electron events and auroral events reported by Schneider et al. (2021) (Section 2.2 and 3). We lastly discuss the broad impact and conclude this study in Section 4.

2. Empirical Criteria for Selecting Auroral Electron Events

2.1. Empirical Criteria

In this section, we establish empirical criteria for selecting electron events that could trigger *detectable* auroral observations by the IUVS instrument. Theoretically, electron precipitation with an energy above the energy threshold (11.5 eV for CO Cameron bands excitation from electron impact on CO_2) should trigger aurorae. However, for detectable auroral emissions, the brightness of CO Cameron bands has to be above the instrument's background level, which is ∼0.5 kR for IUVS. Practically, detectable aurorae are commonly associated with electron acceleration events (e.g., Gérard et al., 2015; Leblanc et al., 2008; Xu, Mitchell, et al., 2020), which suggests high electron fluxes at high energies. Based on simulation results (e.g., Soret et al., 2016, 2021), the primary electron beam should have an energy of ∼50–2,000 eV to cause the auroral emission to peak below ∼150 km altitude, as suggested by IUVS measurements (e.g., Soret et al., 2021). However, the electron flux threshold has not yet been determined to our knowledge, which is the first goal of this study.

Theoretically, the emission rate (p) should be a function of $\sigma_e f(E)n(z)$, where σ_e is the emission cross section of the CO Cameron bands by electron impact, $f(E)$ is the electron number flux at an energy of E, and $n(z)$ is the neutral density at an altitude of z. In other words, the brightness of aurorae (B) should be linearly correlated with p and thus electron number fluxes, to the first order. Traditionally at Earth, the integrated electron energy flux (in mW m^{-2}) is used to study corresponding auroral emissions to compensate for the fact that high energy electrons can produce more photons than low-energie electrons. Through a statistical correlation analysis shown later in Section 2.2, we determine a threshold of integrated electron energy flux of 1.1×10^{10} $eVcm^{-2}s^{-1}sr^{-1}$ (0.018 mW m^{-2} sr^{-1}) over 50–2,000 eV (but not integrated over solid angle).

Another necessary criterion for precipitating electrons to trigger detectable aurorae is that electrons have to be on magnetic field lines connected to the nightside atmosphere on one end and to the source region (e.g., the solar wind or the dayside ionosphere) on the other end. This naturally sets up a requirement of a one-sided loss cone pitch angle distribution, normally identified as an "open-to-night" topology (e.g., Brain et al., 2007, 2020; Weber et al., 2017, 2019, 2020). It is worth noting that the actual magnetic topology might be deviated from this classical definition in the presence of parallel electric fields. For example, one-sided loss cone could be a result of cross-terminator closed loops but not identified as such because ionospheric photoelectron features are not distinguishable after acceleration. For convenience, we refer to such a topology requirement as an "open-to-night" topology hereafter.

To summarize, our empirical criteria include:

1. The integrated electron energy flux over 50–2,000 eV to be $>1.1 \times 10^{10}$ $eVcm^{-2}s^{-1}sr^{-1}$ (or 0.018 mW m^{-2} sr^{-1});
2. An "open-to-night" topology (one-sided loss cone pitch angle distributions).

We apply these criteria to all the SWEA data from 1 December 2014 to 1 April 2020 to select electron events that could trigger detectable aurorae, termed "auroral electrons" hereafter. We select one-sided loss cone distributions by comparing upward and downward electron fluxes to perpendicular electron fluxes within 100–300 eV. More details are described in Weber et al. (2017) and Xu et al. (2019). We limit our search to the nightside (solar zenith angle (SZA) > 95°) and an altitude range of 170–500 km (low altitudes but above the superthermal electron exobase [Xu, Liemohn, et al., 2016]). We have to use a lower SZA cutoff of 95° than $SZA > 105°$ used in Schneider et al. (2021) to guarantee sufficient sampling at local times near the terminator, as electron measurements are made in-situ, unlike remote sensing by IUVS. We have examined statistical trends of auroral electrons using SZA > 105°, which are not statistically different from that using SZA > 95°, other than being noisier.

2.2. Statistical Results

All the selected auroral electron events are mapped in the geographic coordinates in Figure 1b. The location and the brightness of CO Cameron bands of discrete aurorae reported by Schneider et al. (2021) are shown in Figure 1a for a comparison. Figures 1c and 1d show the averaged electron fluxes (averaged in logarithmic values first) and occurrence rates of auroral electron events. The geographic locations of these two types of events are very similar (panels a and b), particularly in terms of both occurring near strong and also weak crustal regions.

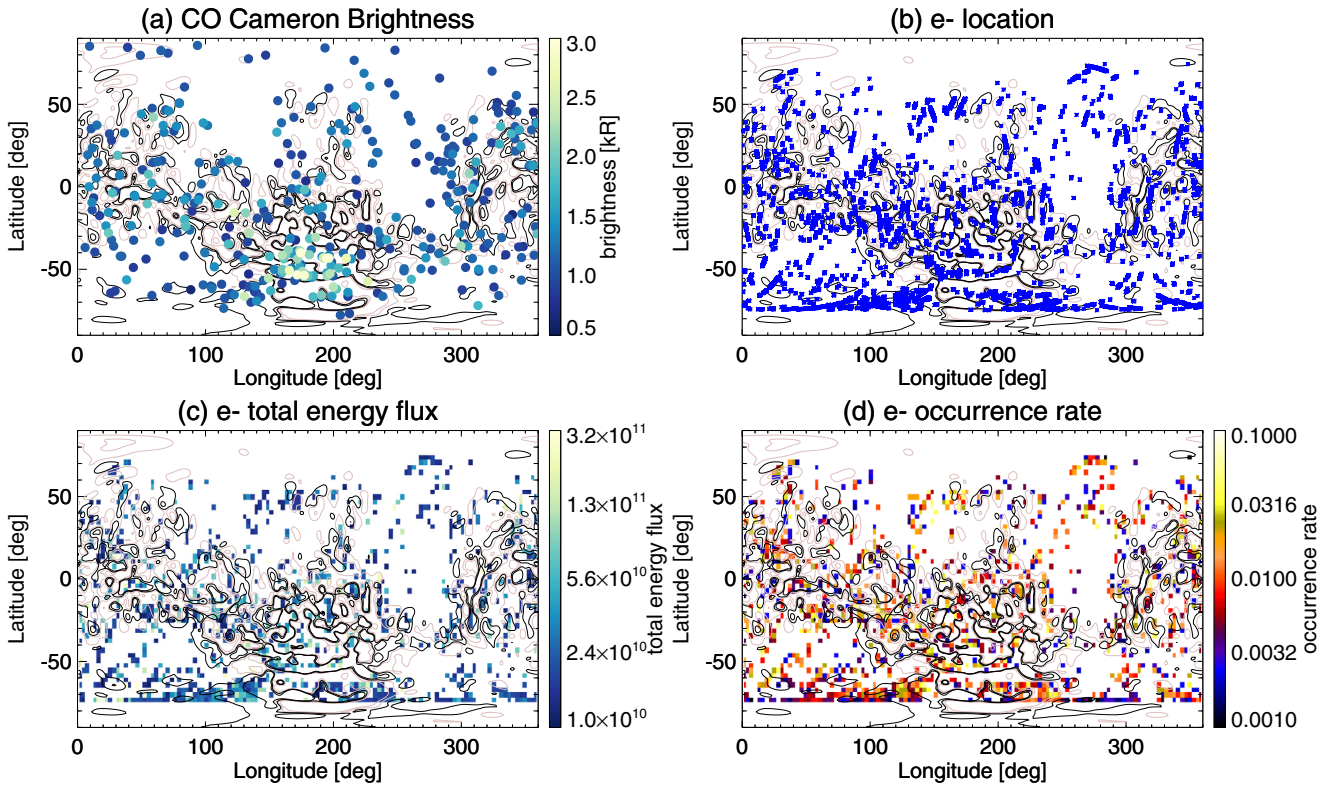

Figure 1. (a) Locations in the geographic coordinates and brightness (color) of discrete aurorae observed by IUVS. (b) Locations of auroral electron events in the geographic coordinates. The integrated electron energy fluxes over 50–2,000 eV (eVcm^{-2}s^{-1}sr^{-1}) (c) and occurrence rates (d) of auroral electron events in the geographic coordinates. A minimum of 2 auroral electron events and a minimum of 30 total electron measurements are imposed in panels c and d, respectively. The gray thick, gray thin, black thin, and black thick contours in all four panel show the radial component of the crustal fields at 170 km (Morschhauser et al., 2014) at [−50, −10, 10, 50] nT.

This finding is consistent with the occurrence of discrete auroral events over weak crustal fields, that is not limited to strong crustal magnetic fields as suggested by previous studies. The main difference in location occurs at high latitudes in the north (remote sensed by IUVS but not in-situ measured by SWEA) and in the south (a cluster of electron events at latitude ∼−75°). The latter is caused by MAVEN "over-sampling" this latitude because of its small spatial area. However, the occurrence rate of electron events (Figure 1d), calculated as the number of auroral electron events divided by the total number of electron measurements in each spatial bin, at latitude ∼−75° is in fact fairly low, not contradicting IUVS results. Meanwhile, the occurrence rate for auroral events reported by Schneider et al. (2021) ranges from 0.001 to a few percent, higher near strong crustal fields. This is consistent with our findings of electron events as shown in Figure 1d, which further validates our empirical selection criteria. Another similarity shared by these two types of events is their intensities, comparing Figures 1a and 1c, both more intense near strong crustal fields. This is expected as we show above that electron fluxes should be roughly linearly correlated to auroral brightness.

Schneider et al. (2021) reveal a positive correlation between the auroral brightness and the radial crustal field strength (based on low-altitude MAVEN measurements obtained below 250 km [Weber et al., 2020]). We reproduce this trend in Figure 2a but with the modeled radial crustal magnetic strength at 170 km altitude ($|Br_{170}|$) (Morschhauser et al., 2014). The median auroral brightness increases from ∼0.8 kR for $|Br_{170}| < 10$ nT to ∼1.5 kR for $|Br_{170}| > 200$ nT, by a factor of ∼2. In Figure 2b, we show the medians (and quartiles) of integrated electron energy fluxes as a function of $|Br_{170}|$ as the black line (and error bars). The median electron flux is $\sim 1.8 \times 10^{10}$ eVcm^{-2}s^{-1}sr^{-1} for $|Br_{170}| < 5$ nT and then increases to $\sim 3 \times 10^{10}$ $eVcm^{-2}s^{-1}sr^{-1}$ for $|Br_{170}| > 100$ nT, also showing a factor of ∼2 enhancement.

To quantitatively compare the two, we overplot the scaled median auroral brightness by a factor of $s_0 = 2.2 \times 10^{10}$ as the red line in Figure 2b, which is in a good agreement with median electron fluxes. This is also how we

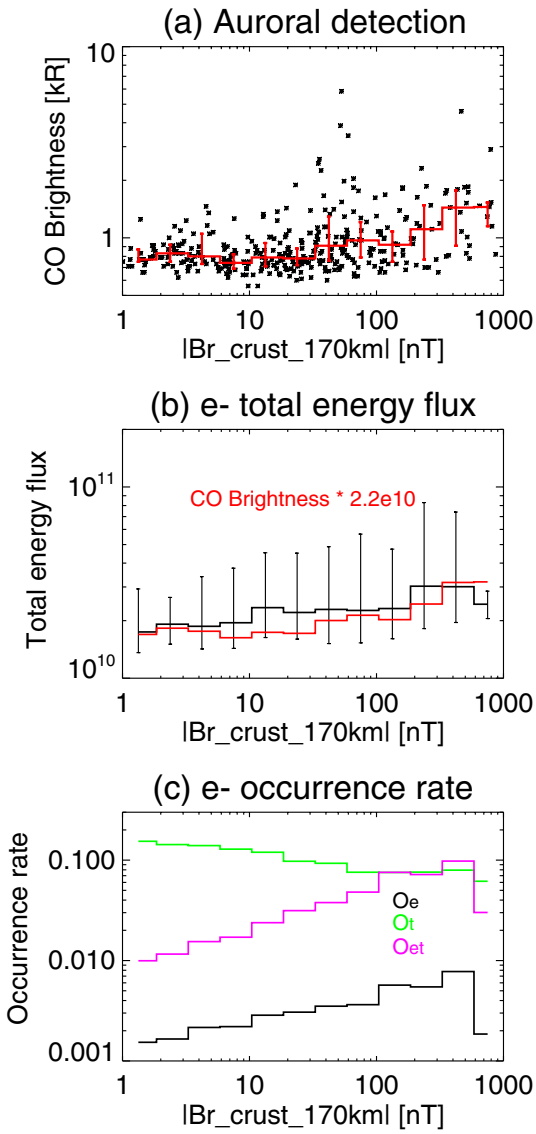

Figure 2. Auroral brightness (a) and integrated electron energy fluxes ($eVcm^{-2}s^{-1}sr^{-1}$) (b) and occurrence rates (c) as a function of $|Br_{170}|$ (Morschhauser et al., 2014). In (a and b), quartiles are shown as red and black lines and errorbars, respectively. The red line in (b) is the median auroral brightness in kR scaled/multiplied by a factor of 2.2×10^{10}. In (c), the black, green, and magenta lines are for O_e, O_t, and O_{et}, respectively.

quantitatively determine the threshold for electron fluxes in an iterative process. More specifically, we apply an electron flux threshold of $t_0 = 0.5s_0$ (0.5 kR being the IUVS detection threshold) and obtain the median electron fluxes as a function of $|Br_{170}|$. We then scale the median auroral brightness by s_0 (the red curve in panel b) to be compared with the median electron flux. We have tested different s_0 until a good agreement between the median electron flux and the scaled median brightness is reached, which gives $s_0 = 2.2 \times 10^{10}$ and $t_0 = 1.1 \times 10^{10}$ $eVcm^{-2}s^{-1}sr^{-1}$. As shown in Figure S1 in Supporting Information S1, our scaling of 2.2×10^{10} $eVcm^{-2}s^{-1}sr^{-1}$ (or 0.036 mW $m^{-2}sr^{-1}$) per kR of CO Cameron bands brightness is in a good agreement with previous studies (Gérard et al., 2015; Leblanc et al., 2008; Soret et al., 2016, 2021). We have additionally tested using electron peak number or energy fluxes within 50–2,000 eV, and integrated number fluxes over 50–2,000 eV, all of which give similar trends with respective thresholds. These thresholds are: 2×10^5 $cm^{-2}s^{-1}sr^{-1}$ eV^{-1} for the peak number flux, 1×10^7 $eVcm^{-2}s^{-1}sr^{-1}$ eV^{-1} for the peak energy flux, and 1×10^8 $cm^{-2}s^{-1}sr^{-1}$ for the integrated number flux.

Schneider et al. (2021) also find an increased occurrence rate for auroral events (O_a) as $|Br|$ increases (not shown here), from ~0.5% to >10%. In comparison, the occurrence rate for auroral electron events (O_e) as a function of $|Br_{170}|$ is shown as the black line in Figure 2c, which is increased from 0.1% to ~0.8%. O_e is lower than O_a, particularly over strong crustal regions, as strong crustal regions are generally closed on the nightside and open field lines are confined in small cusp regions (e.g., Weber et al., 2017; Xu et al., 2019). Locally, however, O_e can be up to ~5%–10% as shown in Figure 1d. We also decompose $O_e = N_e/N_{tot}$ into the occurrence rate of the open-to-night topology (green line, $O_t = N_t/N_{tot}$) and the occurrence rate of auroral electron events on the open-to-night topology alone (magenta line, $O_{et} = N_e/N_t$), also shown in Figure 2c, that is, $O_e = O_t \times O_{et}$, where N_e, N_t, N_{tot} are the sample number of auroral electron observations, electron observations on open-to-night topology, and total electron observations, respectively. O_t remains roughly 10%, varying within a factor of 2 across different $|Br_{170}|$. In contrast, O_{et} has a strong dependence on the crustal strength, increased from 1% to ~10%, which implies the mechanisms that cause the high-energy (50–2,000 eV) electron flux enhancement operate more frequently over strong crustal fields. Also, comparing the variation in O_t and O_{et} against $|Br_{170}|$, the dependence of O_e on $|Br_{170}|$ is mainly driven by O_{et}. In other words, it is the occurrence of electron flux enhancement, rather than the topology variation, that drives the high occurrence of auroral electron events over strong crustal fields.

3. Asymmetries in Auroral Electron Events

A somewhat surprising result from Schneider et al. (2021) is the asymmetry in the occurrence rate of auroral events within a strong crustal field box (30°S − 60°S in latitude and 150°E − 210°E in longitude) in regard to local time (LT) and also the upstream IMF polarity, strongly preferring dusk/pre-midnight ($18 < LT < 24$ hr) and west IMF ($B_y < 0$). In this section, we reveal such preferences also exist in electron events and explore the cause of it. For upstream IMF directions, we use the measured magnetic vectors by the Magnetometer (Connerney et al., 2015) when MAVEN samples the upstream (Halekas et al., 2015, 2017) and otherwise a proxy provided by Ruhunusiri et al. (2018). Magnetic fields in this study are in the Mars-centered Solar Orbit (MSO) coordinate system, where X points from the center of Mars to the Sun, Z points to the north pole of Mars' ecliptic orbit plane, and Y completes the right-handed system.

Figure 3 shows auroral events (left column) and O_e (right column) separated for different conditions: dusk/pre-midnight ($18 < LT < 24$ hr, top row), dawn/post-midnight ($0 < LT < 6$ hr, second row), west IMF ($B_{YMSO} < 0$, third row), and east IMF ($B_{YMSO} > 0$, bottom row). The preference of auroral events inside the highlighted geographic box for dusk ($18 < LT < 24$ hr) and west IMF ($B_{YMSO} < 0$) is reproduced here. Similarly, O_e inside the same geographic box is significantly higher for dusk LTs than dawn LTs and for $B_{YMSO} < 0$ than $B_{YMSO} > 0$. Noticeable differences exist in O_e and auroral events for latitudes $< -60°$, in which total IUVS observations are significantly lower, such that the observational uncertainty in this region is large, in addition to a selection bias in auroral detections near the dawn terminator.

As these auroral events are most likely caused by our selected electron events in a statistical sense, it is not surprising that we find similar trends in both. Meanwhile, as we discussed above, in order to trigger a detectable auroral event, it requires both sufficient electron fluxes and a topology connected to the nightside atmosphere. We explore the cause of preferences in LT and the IMF direction for these two factors separately. Figure 4 shows the occurrence rate of auroral electron events as a function of LT (a) and the IMF clock angle (b) for inside (red) and outside (blue) of the strong crustal field box shown in Figure 3. The clock angle (*bclock*) is defined as the angle from Z_{MSO} to Y_{MSO}, that is, $bclock = \tan^{-1}(B_{YMSO}/B_{ZMSO})$. Similar to the geographic maps in Figure 3, a strong preference of auroral electron events for the dusk LTs (particularly LT 18–21) and $B_{YMSO} < 0$ is seen within the geographic box (red lines in Figures 4a and 4b). In contrast, the occurrence rate outside the box (blue lines) is roughly constant, slightly lower for dusk LTs (a) or IMF in $-ZMSO$ ($bclock = \pm 180°$).

Figures 4c and 4d shows O_t and O_{et} against LT separately for west IMF ($bclock < 0$, magenta) and east IMF ($bclock > 0$, black). In Figure 4c, O_t is highest at dusk LTs and $B_{YMSO} < 0$, up to a factor of 2–3 in LT 19.5–24, implying (spatially and/or temporally) increased paths for electron precipitation. Meanwhile, in Figure 4d, O_{et} is significantly higher for $B_{YMSO} < 0$ than $B_{YMSO} > 0$ for most LTs. For $B_{YMSO} < 0$, O_{et} is highest right past the dusk terminator at LT = 18 hr (~32%) and decreases as the planet rotates, and then raises to ~15% at the dawn terminator. This trend in O_{et} implies the mechanisms responsible for electron flux enhancements, such as inverted-V electron acceleration events (e.g., Brain et al., 2006; Xu, Mitchell, et al., 2020), operate more frequently in the dusk LTs and right at the dawn terminator under west IMFs ($B_{YMSO} < 0$). Also, comparing the variation in O_t and O_{et} against LT, the LT-dependence of O_e within the strong crustal box is mainly driven by O_{et}. It is worth pointing out that these statistical trends within the crustal box may differ if the boundaries of the box are different, especially if more polar-ward crustal fields are also included.

4. Discussion and Conclusions

Previous studies have associated localized auroral observations (termed "discrete aurora") at Mars with electron acceleration events, suggesting high electron fluxes at high energies are needed to trigger the observable aurorae. However, a direct and systematic comparison of these two types of events is hard to make as no simultaneous observations were made. In this study, we establish empirical criteria to select auroral electron events, which allows us to statistically compare the behaviors of these two types of events. Such criteria include (a) the integrated electron energy flux within 50–2,000 eV to be $>1.1 \times 10^{10}$ eVcm^{-2}s^{-1}sr^{-1} (0.018 mW m^{-2} sr^{-1}) and (b) to be on the "open-to-night" topology (one-sided loss cone pitch angle distributions).

Auroral electron events share many statistical similarities to discrete auroral events reported by Schneider et al. (2021). Both electron events and discrete aurorae occur at strong and weak crustal magnetic fields, but not limited to strong crustal fields alone. In addition, Schneider et al. (2021) reveal a positive correlation between the brightness and observational frequency of the auroral events and $|B_r|$. Correspondingly, we find both the occurrence rate and the electron flux of electron events increase with $|B_r|$. These similarities not only validate our selection criteria but also reveal a linear scaling of 2.2×10^{10} eVcm^{-2}s^{-1}sr^{-1} (0.036 mW m^{-2} sr^{-1}) per kR of Cameron bands emission at the limb, which could be applied to other missions such as MEx and Hope.

We also find a dawn-dusk asymmetry in auroral electron events, higher occurrence rates at dusk LTs, as well as a preference for west IMFs, which is consistent with the statistical trends of discrete auroral events (Schneider et al., 2021). We further examine the two selection criteria separately for their impact on the asymmetries. While both factors contribute to the preference of auroral electron events for the dusk terminator and west IMFs, the occurrence rate of auroral electron events on open-to-night topology alone (O_{et}) is the main driver and the

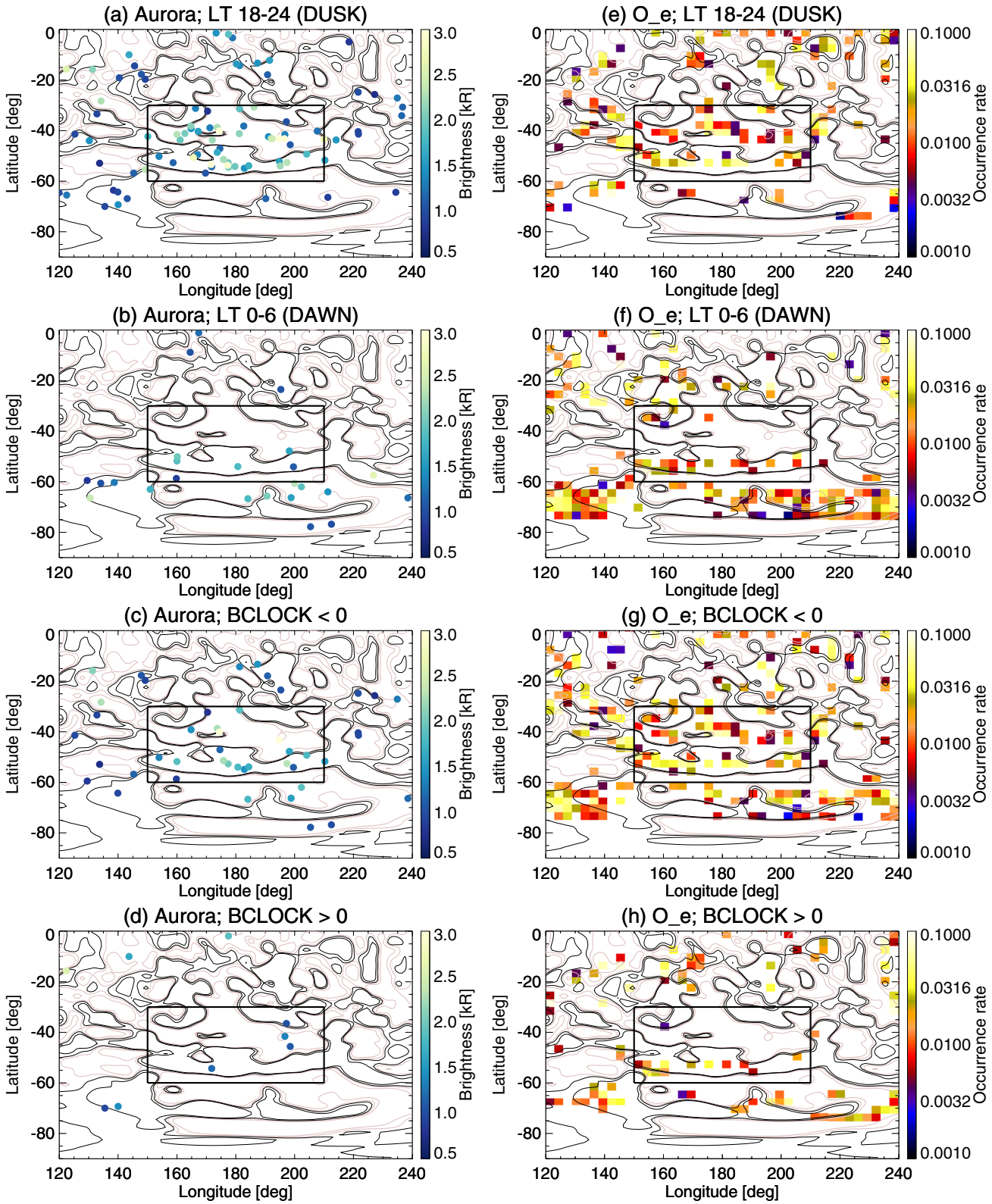

Figure 3. The left column is the location and brightness of auroral events and the right the occurrence rate of auroral electron events, separated from different conditions: dusk/pre-midnight ($18 < LT < 24$ hr, top row), dawn/post-midnight ($0 < LT < 6$ hr, second row), west interplanetary magnetic fields (IMF) ($B_{YMSO} < 0$, third row), and east IMF ($B_{YMSO} > 0$, bottom row).

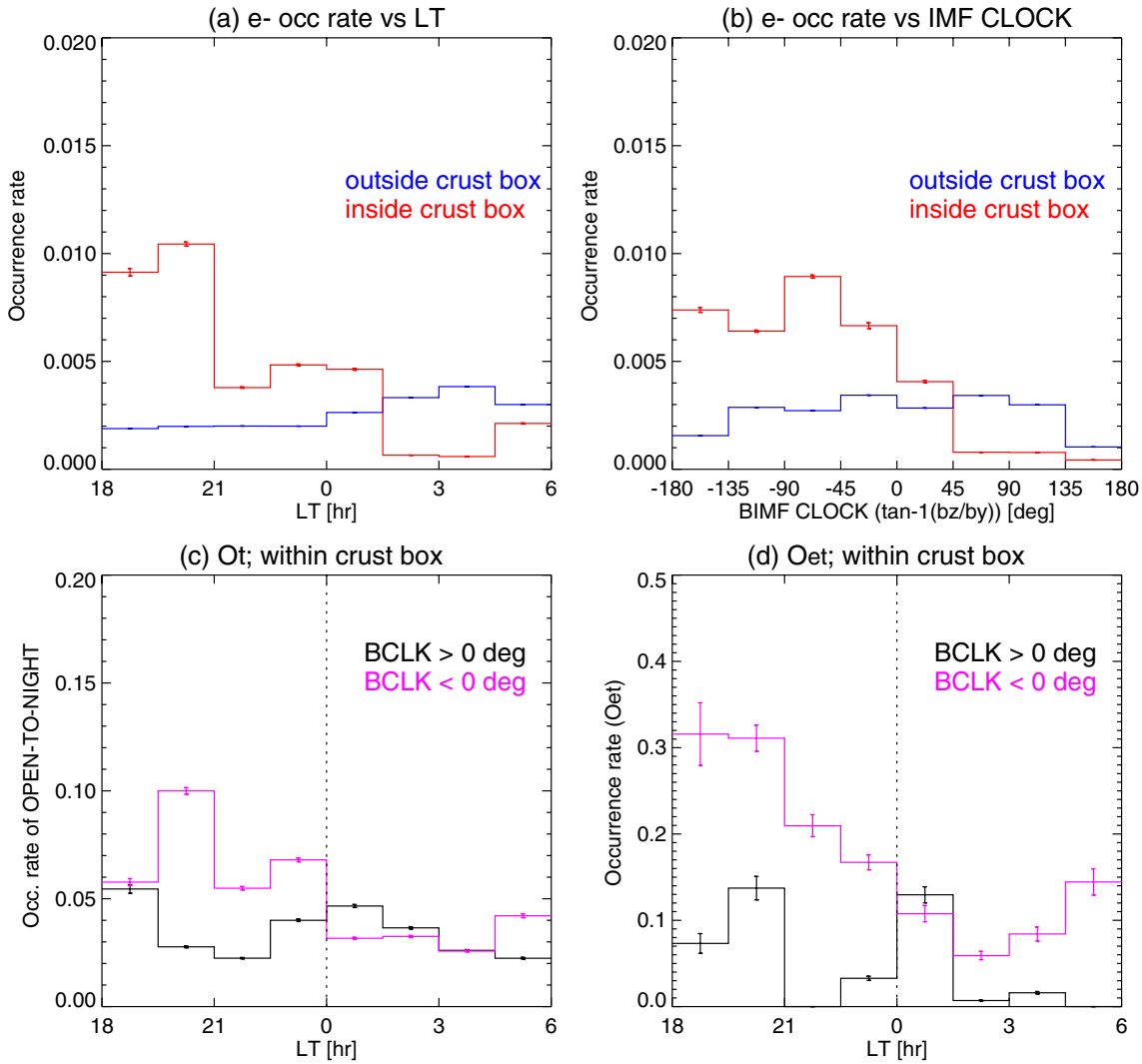

Figure 4. The occurrence rate of auroral electron events as a function of local time (LT) (a) and the interplanetary magnetic fields (IMF) clock angle (b) for inside (red) and outside (blue) of the geographic box shown in Figure 3. Panel (c and d) are O_t and O_{et} against LT, separated for west IMF ($bclk < 0$, magenta) and east IMF ($bclk > 0$, black).

mechanisms responsible for electron flux enhancements operate most frequently near the dusk terminator under west IMFs.

It is also instructive to speculate the source electrons at different regions. The strong preference in LT and upstream IMF orientation within the crustal box suggests these electrons are more likely to be locally accelerated rather than hotter upstream electrons. In contrast, the occurrence of auroral electrons over very weakly magnetized regions might be (partially) attributed to hotter upstream electrons. This study enables future efforts on distinguishing these two types of source auroral electrons by analyzing the electron distribution functions (Akbari et al., 2019), and/or examining the upstream solar wind condition.

In summary, this study provides empirical criteria to select auroral electrons and reveals a linear scaling between the electron flux and auroral brightness, bridging the gap of these two types of observations. It motivates collaborations across different Mars missions, such as joining electron observations from MGS, MEx, and MAVEN, with auroral observations from MEx, MAVEN, and the Hope spacecraft. This study also enables comparative studies of discrete aurorae at different planets, similarities and differences of these auroral emissions at planets with global dipole fields (e.g., Earth and Jupiter) and planets with only localized crustal magnetisms.

Data Availability Statement

The MAVEN data used in this study are available through the Planetary Data System (https://pds-ppi.igpp.ucla.edu/mission/MAVEN). The IUVS limb scan data used in this work is publicly archived on the FAIR-compliant CU (University of Colorado) Scholar Repository at https://doi.org/10.25810/2a0h-9w11.

Acknowledgments
This work was supported by the National Aeronautics and Space Administration (NASA) grant NNH10CC04C to the University of Colorado and by subcontract to Space Sciences Laboratory, University of California, Berkeley. The MAVEN project is supported by NASA through the Mars Exploration Program. Parts of this work for the observations obtained with the SWEA instrument are supported by the French space agency CNES (National Centre for Space Studies). S. Xu and D. L. Mitchell also acknowledge support from NASA's Mars Data Analysis Program, grant 80NSSC17K0455.

References

Akbari, H., Andersson, L., Fowler, C., & Mitchell, D. (2019). Spectral analysis of accelerated electron populations at Mars. *Journal of Geophysical Research: Space Physics*, *124*(10), 8056–8065. https://doi.org/10.1029/2019JA026738

Bertaux, J.-L., Leblanc, F., Witasse, O., Quemerais, E., Lilensten, J., Stern, S., et al. (2005). Discovery of an aurora on Mars. *Nature*, *435*(7043), 790–794. https://doi.org/10.1038/nature03603

Birn, J., Artemyev, A., Baker, D., Echim, M., Hoshino, M., & Zelenyi, L. (2012). Particle acceleration in the magnetotail and aurora. *Space Science Reviews*, *173*(1–4), 49–102. https://doi.org/10.1007/978-1-4614-6455-6_3

Brain, D., Halekas, J., Peticolas, L., Lin, R., Luhmann, J., Mitchell, D., et al. (2006). On the origin of aurora on Mars. *Geophysical Research Letters*, *33*(1). https://doi.org/10.1029/2005gl024782

Brain, D., Lillis, R., Mitchell, D., Halekas, J., & Lin, R. (2007). Electron pitch angle distributions as indicators of magnetic field topology near Mars. *Journal of Geophysical Research*, *112*(A9). https://doi.org/10.1029/2007ja012435

Brain, D., Weber, T., Xu, S., Mitchell, D. L., Lillis, R. J., Halekas, J. S., et al. (2020). Variations in nightside magnetic field topology at Mars. *Geophysical Research Letters*, *47*(19), e2020GL088921. https://doi.org/10.1029/2020GL088921

Connerney, J., Espley, J., Lawton, P., Murphy, S., Odom, J., Oliversen, R., & Sheppard, D. (2015). The MAVEN magnetic field investigation. *Space Science Reviews*, *195*(1), 257–291. https://doi.org/10.1007/s11214-015-0169-4

Fowler, C. M., Agapitov, O. V., Xu, S., Mitchell, D. L., Andersson, L., Artemyev, A., et al. (2020). Localized heating of the martian topside ionosphere through the combined effects of magnetic pumping by large-scale magnetosonic waves and pitch angle diffusion by whistler waves. *Geophysical Research Letters*, *47*(5), e2019GL086408. https://doi.org/10.1029/2019GL086408

Fowler, C. M., Hanley, K. G., McFadden, J. P., Chaston, C. C., Bonnell, J. W., Halekas, J. S., et al. (2021). Maven observations of low frequency steepened magnetosonic waves and associated heating of the Martian nightside ionosphere. *Journal of Geophysical Research: Space Physics*, *126*(10), e2021JA029615. https://doi.org/10.1029/2021JA029615

Gérard, J.-C., Soret, L., Libert, L., Lundin, R., Stiepen, A., Radioti, A., & Bertaux, J.-L. (2015). Concurrent observations of ultraviolet aurora and energetic electron precipitation with Mars Express. *Journal of Geophysical Research: Space Physics*, *120*(8), 6749–6765. https://doi.org/10.1002/2015ja021150

Halekas, J., Brain, D., Lin, R., Luhmann, J., & Mitchell, D. (2008). Distribution and variability of accelerated electrons at Mars. *Advances in Space Research*, *41*(9), 1347–1352. https://doi.org/10.1016/j.asr.2007.01.034

Halekas, J., Ruhunusiri, S., Harada, Y., Collinson, G., Mitchell, D., Mazelle, C., et al. (2017). Structure, dynamics, and seasonal variability of the Mars-solar wind interaction: MAVEN Solar Wind Ion Analyzer in-flight performance and science results. *Journal of Geophysical Research: Space Physics*, *122*(1), 547–578. https://doi.org/10.1002/2016ja023167

Halekas, J., Taylor, E., Dalton, G., Johnson, G., Curtis, D., McFadden, J., et al. (2015). The solar wind ion analyzer for MAVEN. *Space Science Reviews*, *195*(1–4), 125–151. https://doi.org/10.1007/s11214-013-0029-z

Harada, Y., Halekas, J., Xu, S., DiBraccio, G., Ruhunusiri, S., Hara, T., et al. (2020). Ion jets within current sheets in the Martian Magnetosphere. *Journal of Geophysical Research: Space Physics*, *125*(12), e2020JA028576. https://doi.org/10.1029/2020ja028576

Horaites, K., Andersson, L., Schwartz, S. J., Xu, S., Mitchell, D. L., Mazelle, C., et al. (2021). Observations of energized electrons in the martian magnetosheath. *Journal of Geophysical Research: Space Physics*, *126*(4), e2020JA028984. https://doi.org/10.1029/2020JA028984

Leblanc, F., Witasse, O., Lilensten, J., Frahm, R. A., Safaenili, A., Brain, D. A., et al. (2008). Observations of aurorae by SPICAM ultraviolet spectrograph on board Mars Express: Simultaneous ASPERA-3 and MARSIS measurements. *Journal of Geophysical Research*, *113*(A8). https://doi.org/10.1029/2008JA013033

Leblanc, F., Witasse, O., Winningham, J., Brain, D., Lilensten, J., Blelly, P.-L., et al. (2006). Origins of the Martian aurora observed by Spectroscopy for Investigation of Characteristics of the Atmosphere of Mars (SPICAM) on board Mars Express. *Journal of Geophysical Research*, *111*(A9). https://doi.org/10.1029/2006JA011763

Liemohn, M. W., Frahm, R., Winningham, J., Ma, Y., Barabash, S., Lundin, R., et al. (2006). Numerical interpretation of high-altitude photoelectron observations. *Icarus*, *182*(2), 383–395. https://doi.org/10.1016/j.icarus.2005.10.036

Mauk, B. H., Clark, G., Gladstone, G. R., Kotsiaros, S., Adriani, A., Allegrini, F., et al. (2020). Energetic particles and acceleration regions over Jupiter's polar cap and main aurora: A broad overview. *Journal of Geophysical Research: Space Physics*, *125*(3), e2019JA027699. https://doi.org/10.1029/2019ja027699

Mauk, B. H., Haggerty, D., Paranicas, C., Clark, G., Kollmann, P., Rymer, A., et al. (2017). Discrete and broadband electron acceleration in Jupiter's powerful aurora. *Nature*, *549*(7670), 66–69. https://doi.org/10.1038/nature23648

McClintock, W. E., Schneider, N. M., Holsclaw, G. M., Clarke, J. T., Hoskins, A. C., Stewart, I., et al. (2015). The imaging ultraviolet spectrograph (IUVS) for the maven mission. *Space Science Reviews*, *195*(1–4), 75–124. https://doi.org/10.1007/s11214-014-0098-7

Mitchell, D., Lin, R., Mazelle, C., Reme, H., Cloutier, P., Connerney, J., et al. (2001). Probing Mars' crustal magnetic field and ionosphere with the MGS Electron Reflectometer. *Journal of Geophysical Research*, *106*(E10), 23419–23427. https://doi.org/10.1029/2000je001435

Mitchell, D., Mazelle, C., Sauvaud, J.-A., Thocaven, J.-J., Rouzaud, J., Fedorov, A., et al. (2016). The MAVEN solar wind electron analyzer. *Space Science Reviews*, *200*(1–4), 495–528. https://doi.org/10.1007/s11214-015-0232-1

Morschhauser, A., Lesur, V., & Grott, M. (2014). A spherical harmonic model of the lithospheric magnetic field of Mars. *Journal of Geophysical Research: Planets*, *119*(6), 1162–1188. https://doi.org/10.1002/2013je004555

Nakamura, Y., Terada, N., Leblanc, F., Rahmati, A., Nakagawa, H., Sakai, S., et al. (2022). Modeling of diffuse auroral emission at Mars: Contribution of MeV protons. *Journal of Geophysical Research: Space Physics*, *127*(1), e2021JA029914. https://doi.org/10.1029/2021JA029914

Ruhunusiri, S., Halekas, J. S., Espley, J. R., Eparvier, F., Brain, D., Mazelle, C., et al. (2018). An artificial neural network for inferring solar wind proxies at Mars. *Geophysical Research Letters*, *45*(20), 10855–10865. https://doi.org/10.1029/2018GL079282

Schneider, N. M., Deighan, J. I., Jain, S. K., Stiepen, A., Stewart, A. I. F., Larson, D., et al. (2015). Discovery of diffuse aurora on Mars. *Science*, *350*(6261), aad0313. https://doi.org/10.1126/science.aad0313

Schneider, N. M., Jain, S. K., Deighan, J., Nasr, C. R., Brain, D. A., Larson, D., et al. (2018). Global aurora on Mars during the September 2017 Space Weather Event. *Geophysical Research Letters*, *45*(15), 7391–7398. https://doi.org/10.1029/2018GL077772

Schneider, N. M., Milby, Z., Jain, S. K., Gard, J.-C., Soret, L., Brain, D. A., et al. (2021). Discrete Aurora on Mars: Insights into their distribution and activity from MAVEN/IUVS observations. *Journal of Geophysical Research: Space Physics*, *126*(10), e2021JA029428. https://doi.org/10.1029/2021JA029428

Schwartz, S. J., Andersson, L., Xu, S., Mitchell, D. L., Akbari, H., Ergun, R. E., et al. (2019). Collisionless electron dynamics in the magnetosheath of Mars. *Geophysical Research Letters*, *46*(21), 11679–11688. https://doi.org/10.1029/2019GL085037

Shane, A. D., Xu, S., Liemohn, M. W., & Mitchell, D. L. (2016). Mars nightside electrons over strong crustal fields. *Journal of Geophysical Research: Space Physics*, *121*(4), 3808–3823. https://doi.org/10.1002/2015ja021947

Soret, L., Gérard, J.-C., Libert, L., Shematovich, V. I., Bisikalo, D. V., Stiepen, A., & Bertaux, J.-L. (2016). SPICAM observations and modeling of Mars aurorae. *Icarus*, *264*, 398–406. https://doi.org/10.1016/j.icarus.2015.09.023

Soret, L., Gérard, J.-C., Schneider, N., Jain, S., Milby, Z., Ritter, B., et al. (2021). Discrete aurora on Mars: Spectral properties, vertical profiles, and electron energies. *Journal of Geophysical Research: Space Physics*, *126*(10), e2021JA029495. https://doi.org/10.1029/2021ja029495

Weber, T., Brain, D., Mitchell, D., Xu, S., Connerney, J., & Halekas, J. (2017). Characterization of low-altitude nightside martian magnetic topology using electron pitch angle distributions. *Journal of Geophysical Research: Space Physics*, *122*(10), 9777–9789. https://doi.org/10.1002/2017JA024491

Weber, T., Brain, D., Mitchell, D., Xu, S., Espley, J., Halekas, J., et al. (2019). The influence of solar wind pressure on martian crustal magnetic field topology. *Geophysical Research Letters*, *46*(5), 2347–2354. https://doi.org/10.1029/2019gl081913

Weber, T., Brain, D., Xu, S., Mitchell, D., Espley, J., Halekas, J., et al. (2020). The influence of interplanetary magnetic field direction on martian crustal magnetic field topology. *Geophysical Research Letters*, *47*(19), e2020GL087757. https://doi.org/10.1029/2020GL087757

Xu, S., Curry, S. M., Mitchell, D. L., Luhmann, J. G., Lillis, R. J., & Dong, C. (2020). Superthermal electron deposition on the Mars nightside during ICMEs. *Journal of Geophysical Research: Space Physics*, *125*(10), e2020JA028430. https://doi.org/10.1029/2020JA028430

Xu, S., Liemohn, M., Bougher, S., & Mitchell, D. (2016). Martian high-altitude photoelectrons independent of solar zenith angle. *Journal of Geophysical Research: Space Physics*, *121*(4), 3767–3780. https://doi.org/10.1002/2015JA022149

Xu, S., Mitchell, D., Liemohn, M., Dong, C., Bougher, S., Fillingim, M., et al. (2016). Deep nightside photoelectron observations by MAVEN SWEA: Implications for Martian northern hemispheric magnetic topology and nightside ionosphere source. *Geophysical Research Letters*, *43*(17), 8876–8884. https://doi.org/10.1002/2016GL070527

Xu, S., Mitchell, D., Liemohn, M., Fang, X., Ma, Y., Luhmann, J., et al. (2017). Martian low-altitude magnetic topology deduced from MAVEN/SWEA observations. *Journal of Geophysical Research: Space Physics*, *122*(2), 1831–1852. https://doi.org/10.1002/2016JA023467

Xu, S., Mitchell, D., Luhmann, J., Ma, Y., Fang, X., Harada, Y., et al. (2017). High-altitude closed magnetic loops at Mars observed by MAVEN. *Geophysical Research Letters*, *44*(22), 11229–11238. https://doi.org/10.1002/2017GL075831

Xu, S., Mitchell, D. L., Ma, Y., Weber, T., Brain, D. A., Halekas, J., et al. (2021). Global Ambipolar Potentials and Electric Fields at Mars Inferred from MAVEN Observations. *Journal of Geophysical Research: Space Physics*, *126*(12), e2021JA029764. https://doi.org/10.1029/2021JA029764

Xu, S., Mitchell, D. L., McFadden, J. P., Fillingim, M. O., Andersson, L., Brain, D. A., et al. (2020). Inverted-V electron acceleration events concurring with localized auroral observations at Mars by MAVEN. *Geophysical Research Letters*, *47*(9), e2020GL087414. https://doi.org/10.1029/2020GL087414

Xu, S., Schwartz, S. J., Mitchell, D. L., Horaites, K., Andersson, L., Halekas, J., & Gruesbeck, J. R. (2021). Cross-shock electrostatic potentials at Mars inferred from MAVEN measurements. *Journal of Geophysical Research: Space Physics*, *126*(3), e2020JA029064. https://doi.org/10.1029/2020JA029064

Xu, S., Weber, T., Mitchell, D. L., Brain, D. A., Mazelle, C., DiBraccio, G. A., & Espley, J. (2019). A technique to infer magnetic topology at Mars and its application to the terminator region. *Journal of Geophysical Research: Space Physics*, *124*(3), 1823–1842. https://doi.org/10.1029/2018ja026366